glass membranes were produced by Corning (Vycor®), Schott, and PPG. Glass membranes are typically made as discs, tubes or hollow-fibres. To produce microporous glass membranes, a homogeneous melt consisting of 70 wt% SiO_2, 23 wt% B_2O_3 and 7 wt% Na_2O is formed between 1300 to 1500°C. Phase separation of the initially homogeneous glass melt occurs by lowering the temperature to about 800°C. One phase consists primarily of insoluble silicon dioxide. The other phase, rich in alkali borate, can be leached from the heterogeneous glass by treatment with a mineral acid. After removal of the alkali borate phase, a microporous silica membrane is formed.

Future Developments

During the past forty years membranes have gained significant importance in a wide variety of industrial separations. Currently, polymeric membranes are most commonly used for commercial applications. However, recent developments on inorganic membranes are very promising and such membranes may broaden the separation spectrum of membranes for separations. The wide-spread use of inorganic membranes in industrial applications is currently limited by their poor mechanical stability and very high production costs. If these problems can be solved in future work, inorganic membranes will present a new generation of high-performance membranes for the next millennium.

Further Reading

Baker RW, Cussler EL, Eykamp W *et al.* (1991) *Membrane Separation Systems – Recent Developments and Future Directions*. Park Ridge, NJ: Noyes Data Corporation.

Bhave RR (1991) *Inorganic Membranes*. New York: Van Nostrand Reinhold.

Burggraaf AJ and Cot L (1996) *Fundamentals of Inorganic Membrane Science and Technology*. Amsterdam: Elsevier.

Cabasso I (1987) In *Encyclopedia of Polymer Science and Engineering*, Vol. 9, pp. 509–579. New York: John Wiley and Sons.

Kesting RE (1971) *Synthetic Polymeric Membranes*. New York: McGraw-Hill Book Company.

Kesting RE and Fritzsche AK (1993) *Polymeric Gas Separation Membranes*. New York: John Wiley and Sons, Inc.

Koros WJ and Pinnau I (1994) In: Paul DR and Yampolskii YP (eds) *Polymeric Gas Separation Membranes*, pp. 209–271. Boca Raton: CRC Press.

Lloyd DR (1985) *Materials Science of Synthetic Membranes*. ACS Symp. Ser. 269. Washington DC: ACS.

Mulder M (1996) *Basic Principles of Membrane Technology*, 2nd edn, Boston, MA: Kluwer Academic Publishers.

Petersen RJ and Cadotte JE (1990) In: Porter MC (ed) *Handbook of Industrial Membrane Technology*, pp. 307–348. Park Ridge, NJ: Noyes Publications.

Pinnau I (1994) *Polym. Adv. Techn.*, 5, 733.

Strathmann H (1979) *Trennung von molekularen Mischungen mit Hilfe synthetischer Membranen*. Darmstadt: Dr. Dietrich Steinkopff Verlag.

Strathmann H (1990) In: Porter MC (ed) *Handbook of Industrial Membrane Technology*, pp. 1–60. Park Ridge, NJ: Noyes Publications.

Microfiltration

I. H. Huisman, AMKM, TNO Voeding, AJ Zeist, Holland

Introduction

Microfiltration is a separation technique for removing micron-sized particles, like bacteria, yeast cells, colloids, and smoke particles, from suspensions or gases. The process uses membrane filters with pores in the approximate size range 0.1 to 10 μm, which are permeable to the fluid, but retain the particles, thus causing separation. Examples of particles with sizes in the microfiltration range are presented in **Figure 1**.

Microfiltration membranes were first commercialized in the 1920s, and were at that time mainly used for the bacteriological analysis of water. After 1960 the number of successful microfiltration applications grew rapidly, and nowadays microfiltration processes are operated in such different fields as the biotechnological, automobile, electronics, and food industry. Examples of applications are the harvesting of bacterial and yeast cells, the recovery of latex pigments from paints, and the purification of water for the electronics industry. In the food industry, microfiltration is used in the clarification of fruit juices, wine, and beer, in fat removal from whey and in removal of bacteria from milk.

Microfiltration is the largest industrial market within the membrane field, responsible for about 40% of total sales, both in Europe and in the USA. In 1997, the US microfiltration membrane market amassed revenues worth about $400 million, growing at an average annual growth rate of 6.6%. Microfiltration can be carried out in two different operation modes: dead-end (in line) filtration and cross-flow

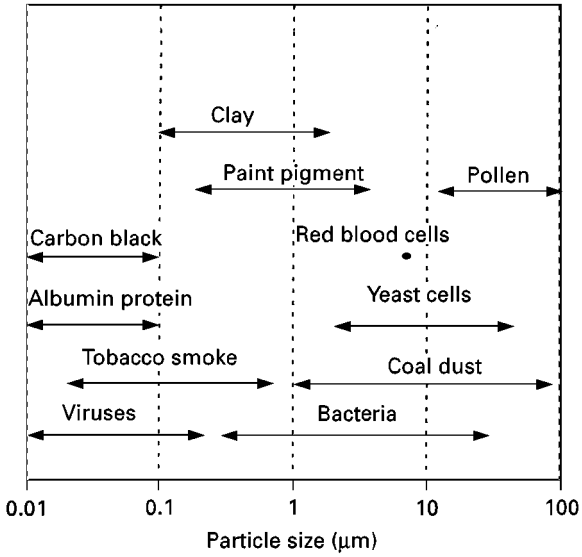

Figure 1 Particles in microfiltration size range.

(tangential flow) filtration (**Figure 2**). In *dead-end filtration* the main flow direction is perpendicular to the membrane. The suspended particles are continuously dragged towards the membrane and deposit on the surface or inside the membrane pores. The deposition of particles leads to a continuously increasing resistance to flow and thus to a continuously decreasing permeate flux rate. To reduce this deposition process, microfiltration is often carried out in the *cross-flow mode* (tangential flow) in which the main flow direction is tangential to the membrane. The flow 'scours' away particles from the membrane surface, and thus limits particle deposition.

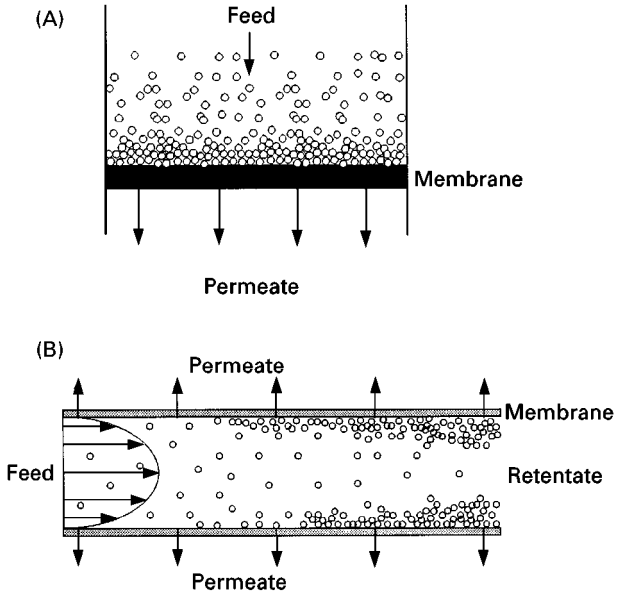

Figure 2 (A) Dead-end filtration and (B) cross-flow microfiltration using a tubular membrane.

Microfiltration Membranes

Two main types of membrane filters exist: *screen filters* and *depth filters*. Screen filters contain capillary-type pores; particles are retained on the membrane surface primarily by a sieving mechanism. Depth filters contain a random, tortuous porous structure; particles are retained through adsorption and mechanical entrapment within the bulk of the filter. Screen filters are absolute: particles larger than the pore size are retained, whereas particles smaller than the pore size can pass relatively easily through the membrane. Particle retention of depth filters is not that clearly defined: retention values increase slowly over a broad particle size range and only reach 100% for very large particles. Depth filters are often used for dead-end filtration, as they can retain a high particle load.

Membrane Materials and Membrane Preparation

Microfiltration membranes are available in a wide variety of materials and methods of manufacture. Many membranes are made of polymers, such as cellulose acetate, polysulfone, and polyvinylidene fluoride (PVDF). Most of these membranes are solvent cast, through a phase inversion process. Other preparation techniques are stretching (polytetrafluoroethylene, PTFE, membranes) and track-etching (polycarbonate membranes). The track-etching process results in cylindrical pores with a very narrow size distribution.

Other microfiltration membranes available are made from glass, from ceramics, such as alumina, titania, and zirconia, and from metals, such as silver and stainless steel. Advantages of these inorganic materials are their higher stability towards extreme process conditions, such as high temperature, extreme pH values, and solvents different than water. Most metal and some ceramic membranes are produced by a sintering process, whereas other ceramic membranes are produced by sol-gel processing or by anodic oxidation. Some novel membranes are prepared by lithographic techniques.

In **Table 1**, a number of different commercial membranes and some of their key properties are presented, and in **Figure 3** SEM (scanning electron microscopy) and AFM (atomic force microscopy) images of some membranes are shown. Note that the membranes shown here are only a fraction of the total number of membrane materials and membrane manufacturers available.

Table 1 Various microfiltration membranes and their water fluxes

Manufacturer	*Trade name*	*Material*[b]	*Preparation method*	*Pore size*[a] (μm)	*Water permeability at* $20^\circ C$ ($L\,m^{-2}\,h^{-1}\,bar$)
US Filter/SCT	Membralox®	α-Al_2O_3	Sintering	0.2	2 000
Anotec	Anopore®	α-Al_2O_3	Anodic oxidation	0.2	3 600
Carbon Lorraine		Carbon	Pyrolysis	0.2	1 500
Tech Sep	Carbosep®	ZrO_2	Sintering	0.14	400
Millipore	Durapore®	PVDF	Phase inversion	0.22	5 900
	Fluoropore®	PTFE	Stretching	0.22	12 000
	MF-Millipore®	Mixed cellulose esters	Phase inversion	0.22	14 400
Osmonics	PCTE	Polycarbonate	Track-etching	0.2	14 600
	PES	Polyethersulfone	Phase inversion	0.2	20 500
	MCS	Mixed cellulose esters	Phase inversion	0.22	15 400
Whatman	Cyclopore®	Polycarbonate	Track-etching	0.2	16 000
Aquamarijn	Microsieve™	Silicon nitride	Photolithography	0.2	87 000

[a]All these membranes are available with pore sizes in large ranges. The pore sizes closest to 0.22 μm are mentioned here to compare water fluxes of the different membranes. [b]PVDF, polyvinylidene fluoride; PTFE, polytetrafluoroethylene.

Membrane Characterization

Originally the main goal in characterization of porous membranes was to determine the pore-size distribution. It has however been realized more recently that membrane surface properties, such as hydrophobicity, zeta potential and surface roughness, play an important factor in fouling and retention properties of membrane processes. Characterization is therefore nowadays performed by various techniques, measuring different structural and physicochemical parameters. The relatively novel technique of AFM microscopy has been shown to provide information on many membrane properties of interest: pore size distribution, surface roughness, and adhesion behaviour. In **Table 2**, various measurement techniques are summarized.

Dead-end Microfiltration

In dead-end filtration, the fluid is forced perpendicularly through the membrane, while all or most of the particles are retained (Figure 2a). If screen filters are used, these particles build a cake layer on the surface, which causes an additional resistance to flow. If depth filters are used, these particles fill the voids within the membrane bulk, and in this way cause an increased resistance. For both types of filters, the increased resistance causes a continuous decline in flux if a constant transmembrane pressure is used (**Figure 4**). After some time, the flux has been reduced to unacceptably low levels, and the membrane has to be cleaned or replaced.

Dead-end filtration is preferred over cross-flow filtration in situations where the concentration of particles to be removed from the fluid is very low, as is the case for sterile filtration in the pharmaceutical industry, for gas cleaning, and for guard-filters positioned as last step in a high-purity water unit. Dead-end filtration is also used in situations where backflush techniques and gas sparging are so effective that the use of a cross-flow is not necessary, as found in some wastewater-treatment plants.

Fluid Flow through Membrane Pores

The capacity of a microfiltration process is expressed as flux, J, which is the volume of permeate passing through the membrane of area A_m and per unit time:

$$J = \frac{1}{A_m}\frac{dV}{dt} \qquad [1]$$

where V is the volume of permeate, and t is time: Most commercial liquid microfiltration processes operate at fluxes of typically about $10^{-4}\,m\,s^{-1}$ ($360\,L\,m^{-2}\,h^{-1}$).

The driving force for this flux is the *transmembrane pressure* (most commonly written as ΔP), the pressure difference between feed side and permeate side, which results from applying either suction to the permeate side or pressure to the feed side, or both. Transmembrane pressures in liquid microfiltration are typically 5–100 kPa (0.05–1 bar). It was found phenomenologically that the flux increases linearly with the transmembrane pressure (Darcy's law):

$$J = \frac{\Delta P}{R_m \cdot \mu_0} \qquad [2]$$

where μ_0 is the permeate viscosity, and R_m is the hydraulic resistance of the membrane against

permeate flow. The *permeability* of the membrane is defined as the inverse of its resistance ($1/R_m$). Microfiltration membranes have permeabilities of typically 10^{-11} m.

The permeability is related to the pore size. The exact relation between permeability and pore size depends on the geometry. For straight cylindrical pores, the Hagen–Poiseuille equation yields:

$$R_m = \frac{8l}{\varepsilon_m r_p^2} \quad [3]$$

where l is the membrane thickness, ε_m is the membrane porosity, and r_p is the pore radius. For membranes comprised of sintered spheres, the Kozeny–Carman equation may give a better approximation:

$$R_m = \frac{45(1-\varepsilon_m)^2 l}{\varepsilon_m^3 a_m^2} \quad [4]$$

where a_m is the radius of the particles that constitute the membrane.

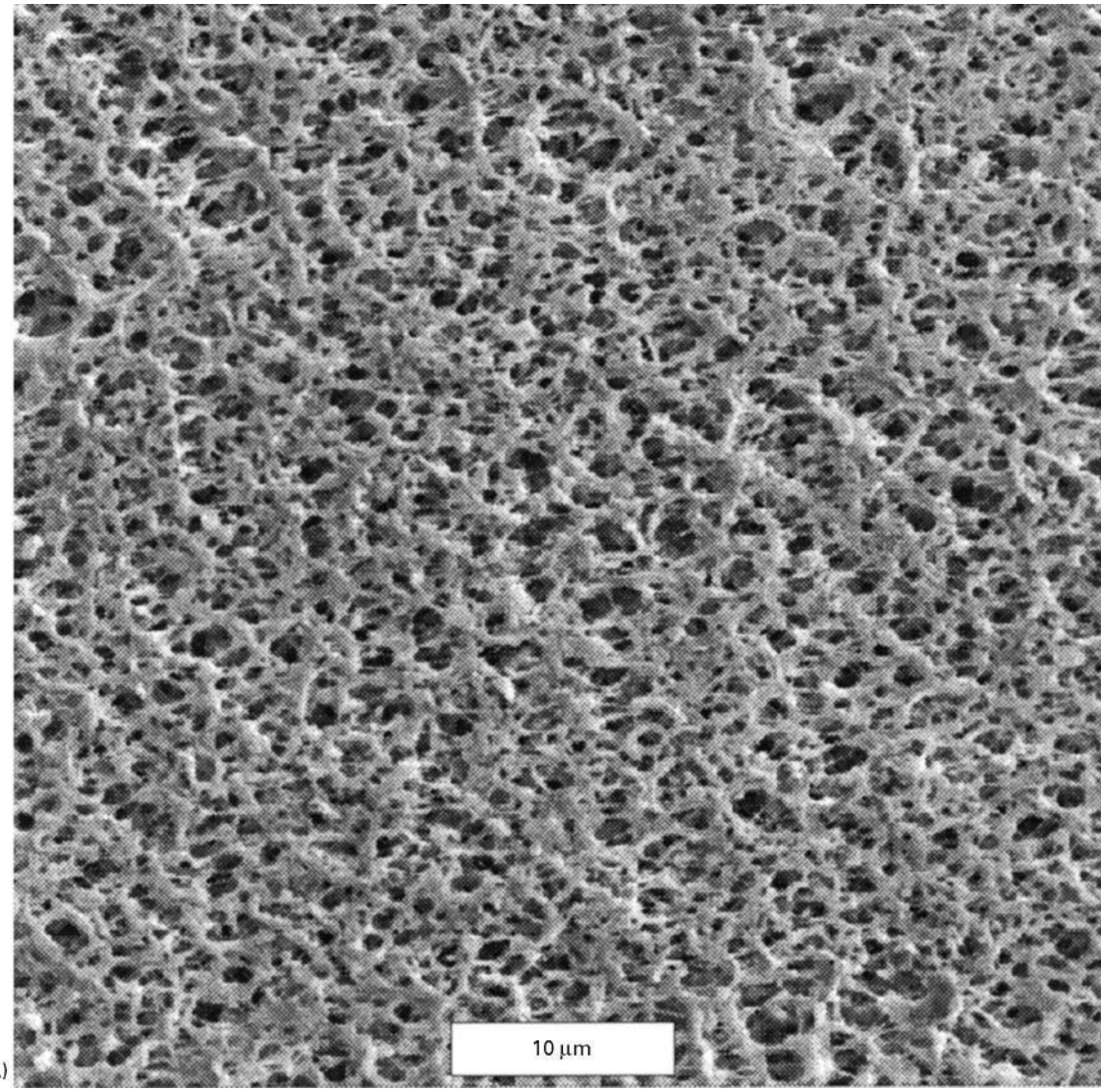

(A)

Figure 3 SEM (A–C, E–H) and AFM (D) of surfaces and cross-section of different membranes. (A) Durapore membrane, rating 0.22 μm, PVDF solvent cast membrane (Millipore). (B) Fluoropore membrane, 0.1 rating, stretched PTFE (Millipore). (C) Polycarbonate track-etched membrane (Osmonics). (D) Anopore membrane, 0.1 μm rating, anodically oxidated Al_2O_3 (Anotec). (E) Microsieve, photolithography, silicon nitride (Aquamarijn). (F) Silver membrane (Millipore). (G) AP15 glass fibre depth filter (Millipore). (H) Cross-section of a P series membrane, solvent cast polyethersulfone (Osmonics). (A), (B), (F) and (G) were kindly supplied by the Millipore corporation. (C) and (H) were kindly supplied by Osmonics; (D) was kindly supplied by the Group of Membrane Science and Technology, University of Valladolid, Spain; (E) was kindly supplied by Aquamarijn.

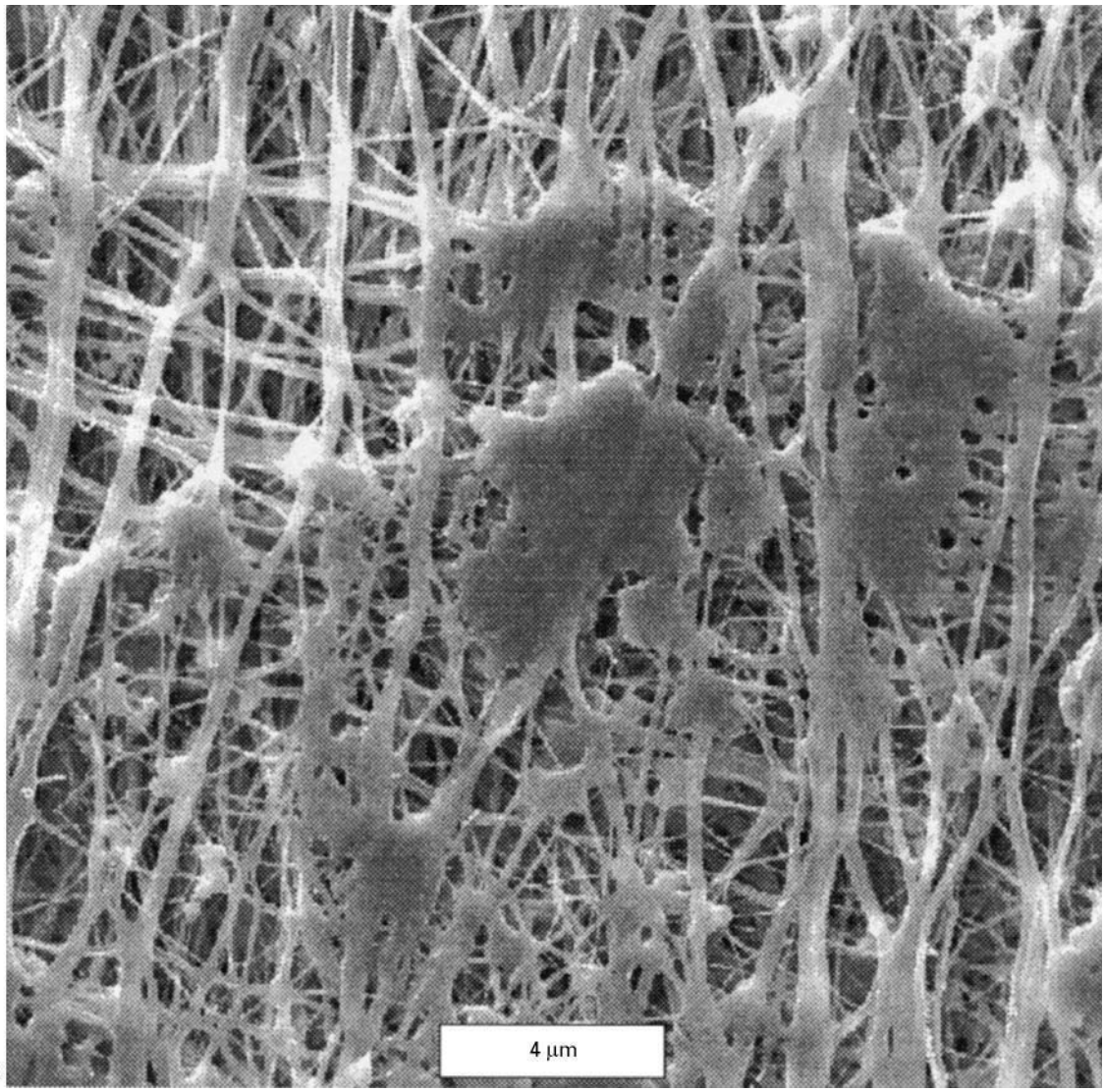

(B)

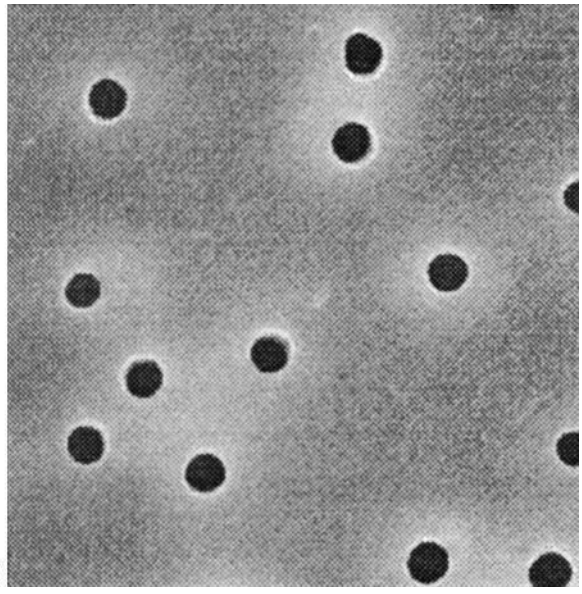

(C)

Figure 3 *Continued*

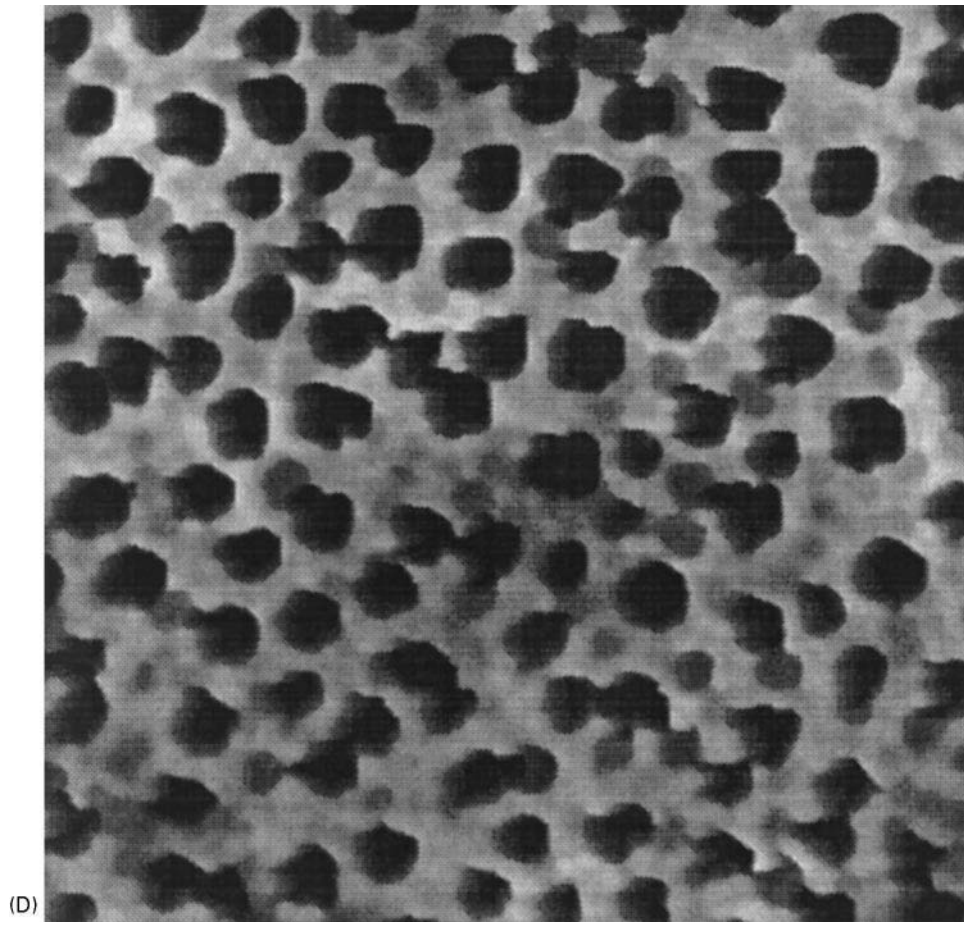

Figure 3 *Continued*

Screen Filters: Cake-layer Build-up

The flux calculated by eqns [2]–[4] is the so-called 'pure water flux'. During filtration, fouling and cake-layer build-up continuously decrease the flux to values much lower than the pure water flux. Darcy's law (eqn [2]) can be written for a fouled membrane as:

$$J = \frac{\Delta P}{R_{tot} \cdot \mu_0} \qquad [5]$$

where R_{tot} is the total hydraulic resistance. It can be divided into the membrane resistance (R_m), the resistance caused by fouling (R_f), and the resistance caused by the cake layer (R_{cake}):

$$R_{tot} = R_m + R_f + R_{cake} \qquad [6]$$

Fouling can be caused by processes such as the adsorption of macromolecules or bacteria. It is difficult

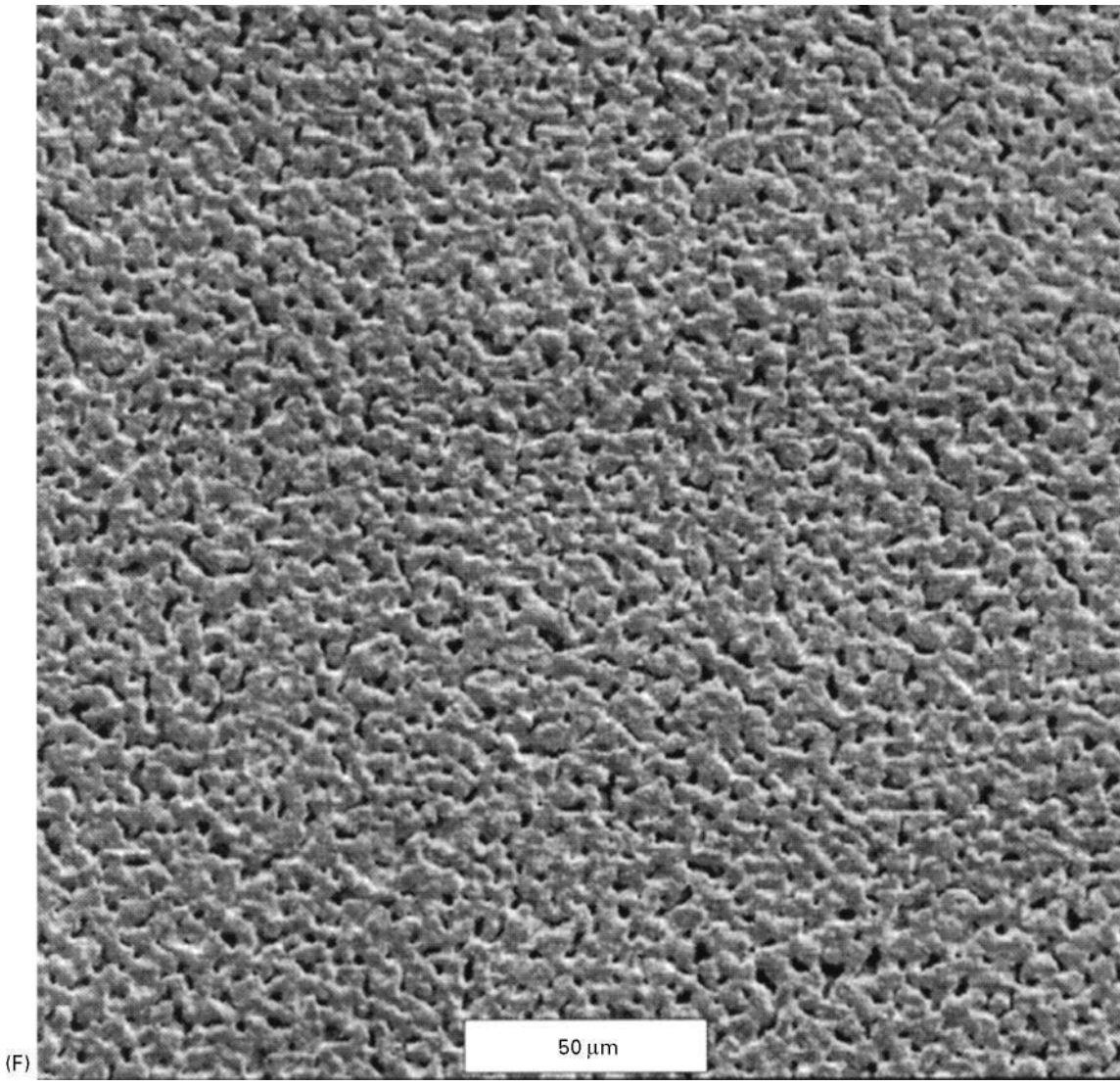

Figure 3 *Continued*

to predict the extent of fouling quantitatively; a qualitative description is given in a later section. The cake resistance can be calculated by the Kozeny–Carman equation, eqn [4], where the cake's void fraction ε, the cake-layer thickness δ_c, and the particle radius a are to be inserted for ε_m, l and a_m respectively.

The void fraction of the cake layer, ε, may depend on various parameters, such as transmembrane pressure, particle size distribution, shape, and compressibility, and the effect of particle–particle interactions. Often a value between 0.3 and 0.4 is found for ε.

A model for the time dependent dead-end filtration flux is obtained by combining eqns [4]–[6] with a mass balance describing cake layer build-up:

$$\left(\frac{d\delta_c}{dt} + J\right)\phi_b = (1-\varepsilon)\frac{d\delta_c}{dt} \qquad [7]$$

where ϕ_b is volume fraction of particles in the bulk.

If a constant ΔP is applied, the flux is given by:

$$J(t) = \frac{\Delta P}{\mu_0 R_m}\left(1 + \frac{2\hat{R}_c\phi_b\Delta P \cdot t}{(1-\varepsilon-\phi_b)\mu_0 R_m^2}\right)^{-1/2} \qquad [8]$$

where $\hat{R}_c$ is the specific cake resistance ($=R_c/\delta_c$). Care must be taken when using eqn [8] as ε and $\hat{R}_c$ often depend on time (cake compaction).

Depth Filters

Particle retention in depth filters is based on various mechanisms. In the case of gas cleaning, the two

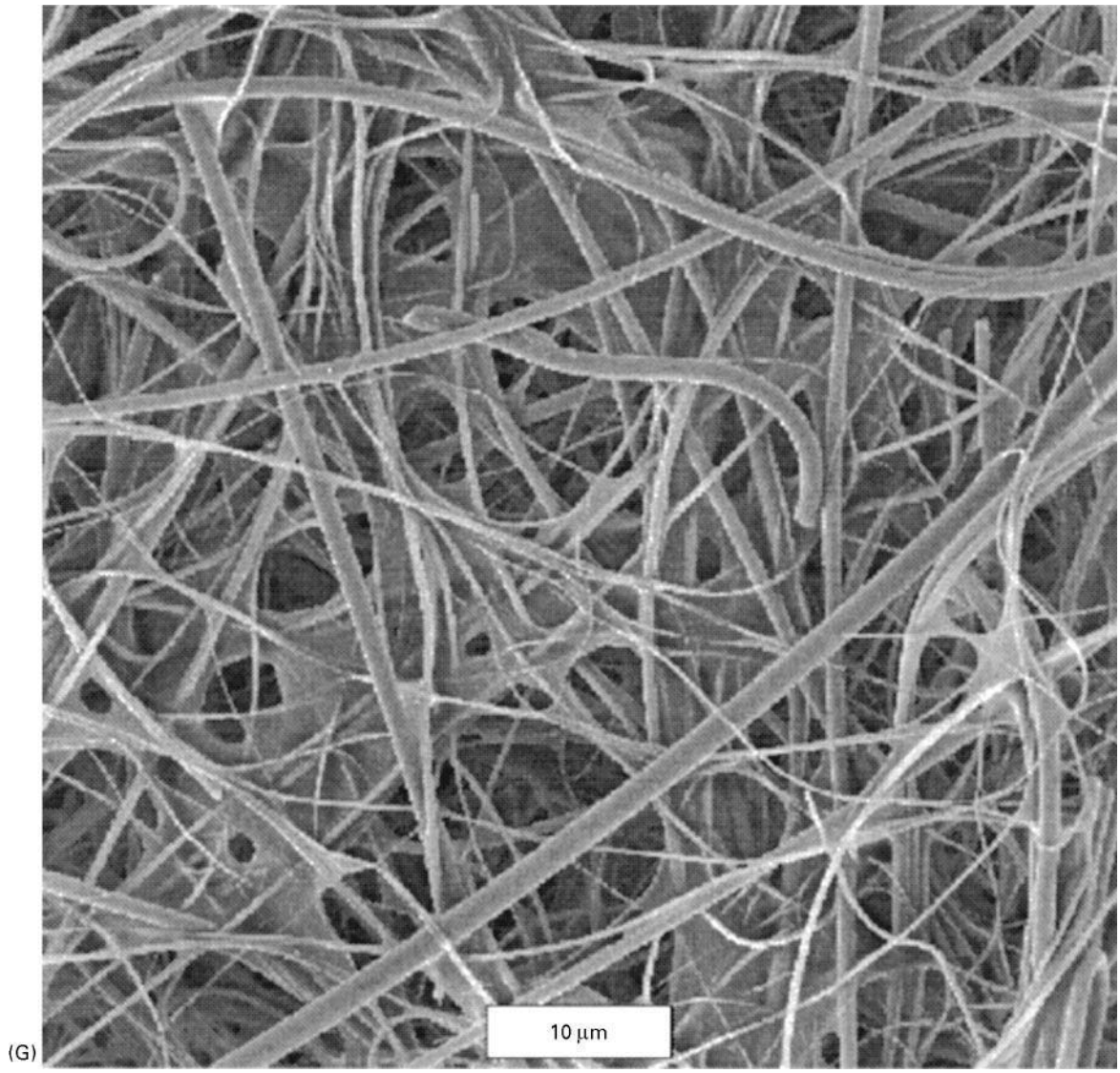

Figure 3 *Continued*

most important mechanisms are particle capture by *interception* and particle capture by *diffusion*. Interception occurs when a particle follows a fluid streamline, which at some point passes close to the filter surface at a distance less than the particle radius, thus causing contact between the particle and the filter.

Table 2 Membrane characterization methods

Method[a]	*Parameters obtained*	*Description/remarks*
Microscopic techniques		'Direct' observation by microscopes.
SEM, TEM, FESEM (+ image analysis)	Pore-size distribution, pore morphology (surface roughness)	Although these methods have many advanced possibilities, they are mostly used for determining the pore-size distribution in the membrane surface. Preparation of sample necessary
AFM (+ image analysis)	Pore-size distribution, morphology, surface roughness, particle–membrane interactions	See SEM (no preparation technique is necessary)
Liquid penetration methods		Liquids will fill larger pores at low pressures. To fill smaller pores, however, higher pressures are needed
Bubble point method	Largest pore available	Simple method, contact angle of membrane–liquid needs to be known
Extended bubble point method	Pore-size distribution	See bubble point method
Mercury porometry	Pore-size distribution	High pressures are necessary that may damage the membrane structure
Permporometry	Pore-size distribution	Vapour condensation in pores is measured. Rather complicated method
Solute retention	Pore-size distribution ('cut-off')	Membranes with smaller pores retain solutes of smaller sizes. Simple method. More often used for ultrafiltration than for microfiltration
Contact angle measurements		
Sessile drop, Wilhelmy plate	Contact angle, surface tension, hydrophobicity	Direct methods that measure the contact angle liquid–air–membrane. Give qualitative infomation on hydrophobicity
Electrokinetic methods		
Electroviscous method	Zeta potential, surface charge density	Experimentally simple: measurement of water flux at various ionic strengths. Interpretation of results more difficult
Streaming potential, electroosmosis	Zeta potential, surface charge density	Direct measurements of electrokinetic effects. Interpretation of results sometimes complicated

[a]SEM, scanning electron microscopy; TEM, transmission electron microscopy; FESEM, field effect scanning electron microscopy; AFM, atomic force microscopy.

Capture by diffusion occurs when the Brownian motion of the particle results in contact between the particle and the filter matrix.

Interception is the dominant capture mechanism for large particles; Brownian diffusion is the dominant capture mechanism for smaller particles. Capture is therefore least effective for intermediate size particles, leading to the existence of a 'most penetrating particle size' (**Figure 5**). The exact value of this most penetrating particle size depends on the membrane pore diameter and the flow velocity. It has been found, however, that capture of particles from gas streams by membranes of pore diameters of about 0.2 μm is so effective that essentially all particles are retained.

For depth filtration of liquids, the situation is different, as physicochemical (charge) effects alter the relative magnitudes of the capture mechanisms described above. If physicochemical conditions are favourable, capture efficiencies in liquids can be similar to those in gases. If conditions are less favourable, capture efficiencies for the smaller particles decrease rapidly. Under these conditions sieving (entrapment) is the only effective particle capture mechanism, making the membrane permeable for all particles smaller than the pore size.

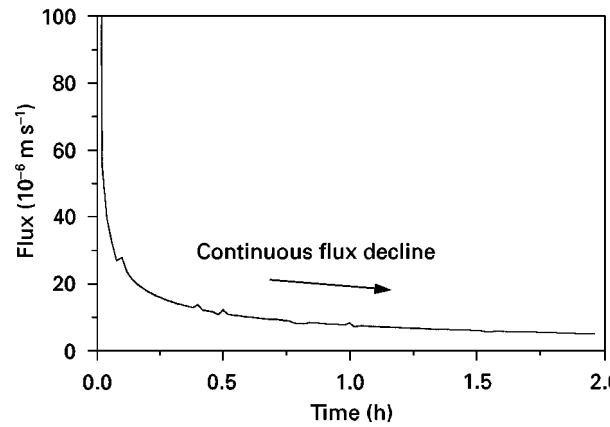

Figure 4 Flux versus time for the dead-end microfiltration of a silica particle suspension.

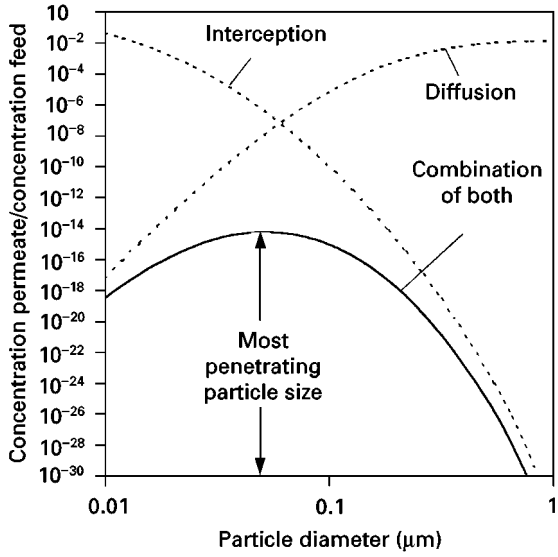

Figure 5 Schematic representation of efficiency of capture by interception and capture by diffusion versus particle size. The most penetrating particle size is obtained by combining both mechanisms.

Cross-flow Microfiltration

Dead-end microfiltration, as stated, may suffer from dramatic flux loss because of deposition of particles on the membrane surface and fouling phenomena. Therefore microfiltration is often carried out in the *cross-flow* mode (Figure 2b). The tangential flow (cross-flow) 'scours' away particles from the membrane surface, and thus limits cake-layer build-up and fouling. Another advantage of cross-flow filtration is the possibility for continuous operation. Cross-flow filtration is used in most industrial large-scale microfiltration plants. For cross-flow microfiltration, screen filters are mainly used.

Cake-layer Build-up and Fouling

During a cross-flow microfiltration process, a flux behaviour is often observed as shown in **Figure 6**. The flux declines at first rapidly with time; then the speed of flux decline decreases, and finally a *steady state* is reached where the flux does not decrease anymore. The decrease in flux is commonly ascribed to two phenomena: *cake-layer build-up* and *fouling*.

When filtering a suspension, the membrane retains suspended particles. The particle concentration near the membrane will therefore gradually increase. Cake-layer build-up will occur when the particle concentration near the membrane surface reaches the maximum packing density (0.6–0.7). Cake-layer build-up is thus caused by the particles that are retained by the membrane based on their size, independent of any specific interaction between these particles and the membrane. Cake-layer build-up in microfiltration is a phenomenon similar to *concentration polarization* in ultrafiltration.

Fouling, on the other hand, is based on a direct contact between solutes and the membrane surface. The term 'fouling' includes many processes, such as adsorption and deposition of macromolecules, bacteria, or small organic molecules on the membrane surface or within the pores. Fouling increases the hydraulic resistance against permeate flow, and thus reduces the capacity of the microfiltration process. Moreover, fouling in general increases the observed retention of the membrane as it reduces the effective pore size.

If one plots the steady-state flux for crossflow microfiltration versus transmembrane pressure (ΔP) often a curve as given in **Figure 7** is obtained. Three regimes can be observed. For low values of ΔP, the flux increases linearly with ΔP and often equals the pure water flux. For higher values of ΔP, the flux curve bends, because of cake-layer build-up, and fluxes become less than the pure water flux. The point where the deviation from the straight line starts is often referred to as the *critical flux*. For even higher ΔP, the flux is independent of the pressure. This pressure independent flux value is referred to as the *limiting flux*.

Factors Influencing Membrane Fouling and Cake-layer Build-up

The extent of membrane fouling and cake-layer build-up depends on many parameters, which can be grouped in three main contributors:

- properties of the membrane,
- properties of the suspension, and
- properties of the process (hydrodynamics).

Membrane properties of importance are hydrophobicity, surface charge (zeta potential), surface

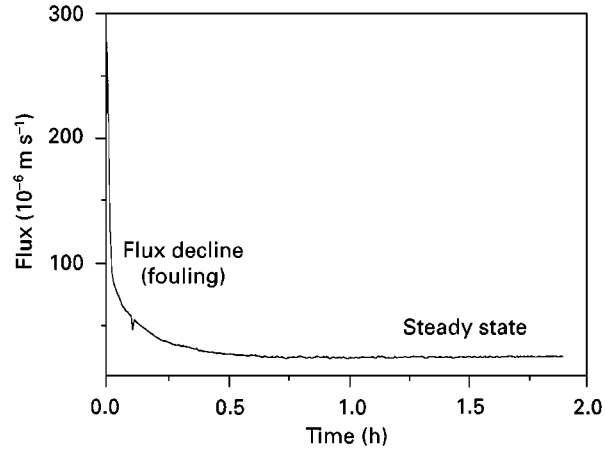

Figure 6 Flux versus time for the cross-flow microfiltration of a silica particle suspension.

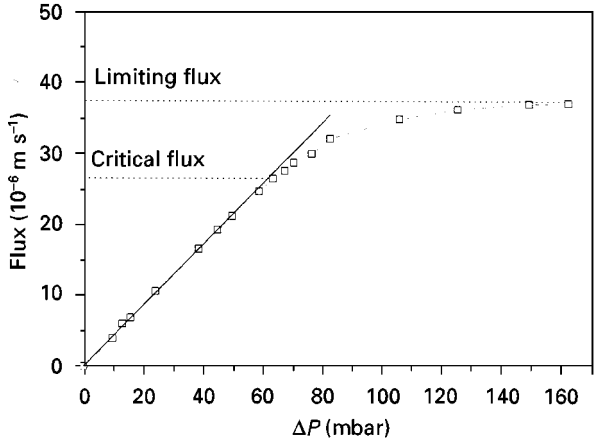

Figure 7 Steady-state flux versus ΔP for the cross-flow microfiltration of a silica particle suspension. ——, water; - - - □ - - -, silica particle suspension.

roughness, and pore-size distribution. In general, macromolecular adsorption is more severe for *hydrophobic* than for hydrophilic membranes. Fouling by negatively charged colloids is less for *negatively charged membranes* than for uncharged or positively charged membranes. As most colloids in practical suspensions acquire a negative charge, negatively charged membranes are preferred in general. Membrane fouling is further reduced by choosing membranes with *smooth surfaces*, small pore sizes, and *narrow pore size distributions*.

Feed suspension properties of importance are particle concentration, particle charge (zeta potential), ionic strength, and overall composition. The amount of cake-layer build-up increases with *particle concentration*. *Charge effects* can reduce fouling by membrane-particle repulsion, and can reduce cake-layer build-up by particle–particle repulsion. Such charge effects are less pronounced at high *ionic strength*, as the ions present in solution 'shield' the charge of membrane and particles. Overall composition of the feed suspension is of great importance for the fouling behaviour. Fouling may be caused not only by the main particles retained, but also by macromolecules and small organic molecules, which 'geometrically' should pass through the pores easily.

Process properties of importance are the transmembrane pressure and the cross-flow velocity. Low fouling normally occurs at low *transmembrane pressures* and high *cross-flow velocities*. More detailed information is given in a later section.

Calculating the Limiting Flux

To calculate the limiting steady-state flux, local mass balances near the membrane surface are used. It is then assumed that the limiting flux is reached when the amount of particles transported *towards* the membrane by the permeate flux (convection) equals the amount of particles transported *away* from the membrane by the cross-flow. The cross-flow can cause back-transport by at least four different mechanisms:

- Brownian diffusion,
- shear-induced diffusion,
- inertial lift, and
- surface transport.

In the following, these mechanisms will be explained. It is assumed throughout this section that the particles are spherical and monodisperse, and that long-term fouling and physicochemical interactions are negligible.

Brownian diffusion If back-transport is caused by Brownian diffusion the standard concentration polarization theory can be used, employing the Brownian diffusion coefficient for spherical particles:

$$D = \frac{kT}{6\pi\mu_0 a} \qquad [9]$$

where k is the Boltzmann constant, T is temperature, and a is the particle radius. By numerical calculations, using a suspension viscosity that depends on the particle concentration, it can be shown that the flux is given by:

$$J = 0.0769\left(\frac{\tau_w k^2 T^2}{\mu_0^3 a^2 L}\right)^{1/3} \phi_b^{1/3} \qquad [10]$$

where τ_w is the wall shear stress and L is the membrane length.

Eqn [10] predicts fluxes of the right order of magnitude for suspensions of small particles (up to about 10 nm). It under-predicts fluxes by one or two orders of magnitude if applied to suspensions of larger particles. This discrepancy is called the 'flux paradox'. This paradox is explained by assuming that there are other mechanisms for back transport, apart from Brownian diffusion.

Shear-induced diffusion When a shear field is applied to a layer of particles, the particles will tumble over one another, leading to a more loosely packed layer. Obviously the particles must move perpendicular to the applied shear stress to achieve this. The resulting particle migration can be described by employing an effective diffusion coefficient, and is called *shear-induced diffusion*.

It can be calculated, using an empirical value of the shear-induced diffusion coefficient, that the limiting flux is given by:

$$J = 0.060 \frac{\tau_w}{\mu_0} \left(\frac{a^4(1 - 3.8\phi_b)}{\phi_b L} \right)^{1/3} \quad [11]$$

valid for $\phi_b < 0.2$, i.e. for all practical applications. Eqn [11] has been shown to give good flux predictions for suspensions of hard spherical particles, and reasonable flux predictions for complex biofluids such as milk. Although eqn [11] is derived for local viscous flow, flux calculations have also been reported to be accurate for many *turbulent* flow processes.

Inertial lift If a diluted suspension of particles flows through a duct, particles present close to the wall will migrate towards the centre, perpendicular to the streamlines. This migration, caused by complex hydrodynamic interactions, is called inertial lift. In cross-flow microfiltration, inertial lift may be able to prevent particles from depositing onto the membrane. To model this phenomenon, it is assumed that a cake layer builds up during microfiltration until the convective velocity *towards* the membrane (the flux J) equals the lift velocity, v_L, *away* from the membrane:

$$J = v_L = 0.036 \frac{\rho_0 a^3 \tau_w^2}{\mu_0^3} \quad [12]$$

The inertial lift theory neglects the influence of a particle on the motion of another particle, resulting in a flux equation which does not depend on the particle concentration. The inertial lift model is therefore only valid for very low particle concentrations. As the flux predicted by eqn [12] increases with the cube of the particle size and the square of the wall shear stress, inertial effects are expected to be important only for large particles (> 5 μm) and high cross-flow velocities ($\tau_w > 10$ N m^{-2}).

Surface transport A particle on top of a filter cake is subject to different forces, as shown in **Figure 8**. The horizontal drag force caused by the cross-flow F_τ exerts a clockwise torque on the particle, and the vertical drag force caused by the permeate flux F_J exerts a counterclockwise torque. If the torque caused by the cross-flow is larger than the torque caused by the permeate flux, the particle can *roll* over the cake layer to the outlet of the membrane. This mechanism of transport is called surface transport.

Equating the clockwise torque with the anticlockwise torque, an equation for the limiting flux is obtained:

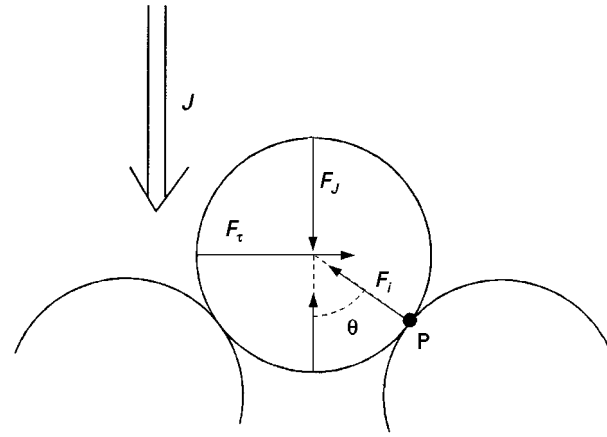

Figure 8 Torque balance for the surface transport model. F_τ = horizontal drag force caused by the cross flow; F_J = vertical drag force caused by the permeate flux J; F_i = particle–particle interaction force; θ = angle of repose.

$$J = \frac{2.36 a \tau_w}{\mu_0 \tan\theta (a^2 \hat{R}_c)^{2/5}} \quad [13]$$

where θ is the angle of repose (see Figure 8).

Just as for the inertial lift model, the present model neglects the influence of a particle on the motion of another particle, resulting in a flux equation which does not depend on the particle concentration. Eqn [13] overpredicts fluxes for typical microfiltration conditions by an order of magnitude or more.

Two of the models described above, the Brownian diffusion model and the shear-induced diffusion model, use a *continuum approach*. The other two, the inertial lift model and the surface transport model, are based on a *single-particle approach*. The single-particle approach is only valid for low particle concentrations and large particles.

In **Figure 9**, the fluxes predicted by the two continuum models are given as a function of particle size for typical cross-flow microfiltration conditions. The flux predicted by the inertial lift model is plotted in the same graph to indicate the order of magnitude of inertial effects. For small particle sizes, Brownian effects dominate and the flux decreases with particle size. For intermediate particle sizes, shear-induced diffusion dominates and the flux *increases* with particle size. For large particle sizes (> 5 μm) inertial effects dominate causing the flux to increase even faster with particle size.

The combined effect of Brownian and shear-induced diffusion can be described by:

$$J_{Bo+SI} = \sqrt{J_{Bo}^2 + J_{SI}^2} \quad [14]$$

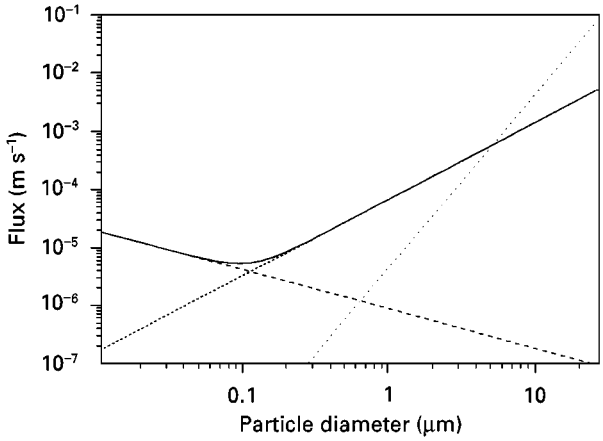

Figure 9 Flux calculated according to different models as a function of particle diameter. Calculations were performed for $\tau_w = 32\ N\ m^{-2}$, $\phi_b = 10^{-3}$, and $L = 1.2\ m$, using eqns [10]–[12] for the Brownian, shear-induced, and inertial-lift models, and using eqn [14] for combining Brownian and shear-induced diffusion, - - - -, Brownian diffusion model; · · · · · ·, shear-induced diffusion model; —, Brownian and shear-induced diffusion model; ⋯ ⋯, inertial lift model.

where J_{Bo} is the flux according to Brownian theory, eqn [10], and J_{SI} is the flux according to shear-induced theory, eqn [11]. Predictions according to eqn [14] are also given in Figure 9.

Calculating the Transient Behaviour of Cross-flow Microfiltration

The time dependence of the flux can be predicted using an approach as outlined in the section on dead-end filtration, yet allowing for back-transport according to the particle transport mechanisms described above. Such descriptions are rather complicated, and will not be treated here.

A simple but effective approach to model the transient behaviour of the permeate flux is the use of a combination of transient dead-end filtration theory and a cross-flow filtration model for the steady-state (limiting) flux. While the cake is initially developing, the effect of the cross-flow is small and can be neglected, so that cross-flow filtration theory can be approximated by dead-end filtration theory. Upon approaching the steady state, the cross-flow begins to arrest the cake growth and dead-end filtration theory is no longer accurate. However, near the steady state the flux shows only minor time dependence, and the flux can be approximated by its steady-state value.

The procedure to predict the total transient behaviour of the permeate flux is thus to use dead-end filtration theory (see the section on dead-end microfiltration) until the time the steady-state flux is reached and then use the steady-state flux predicted by a steady-state cross-flow filtration model. This approach is illustrated in **Figure 10**, modelling the transient flux and cake-layer build-up in the cross-flow microfiltration of a suspension of silica particles.

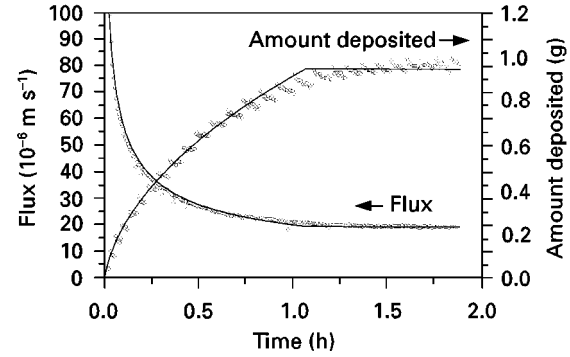

Figure 10 Flux and amount of matter deposited on the membrane as a function of time for the filtration of a suspension of 0.48-μm silica particles. Circles represent experimental values for a particle concentration of 1.7 kg m^{-3}, a transmembrane pressure of 0.42 bar and a cross flow velocity of 1 m s^{-1}; lines represent model calculations.

Process Considerations

Cross-flow microfiltration is usually carried out in the feed-and-bleed mode, shown in **Figure 11**. The use of a retentate recycle makes it possible to work at high cross-flow velocities (high Q_c) while having low retentate flows (i.e. high volumetric concentration factors $V_c = 1 + Q_P/Q_R$). When high concentration factors are desired, several recirculation loops may be placed in series, or in even more complicated schemes, with loops both in parallel and in series (Christmas tree design).

In many cross-flow microfiltration systems and in some dead-end systems, *backflushing* is applied to remove the fouling layer from the membrane. Backflushing is achieved by forcing the permeate periodically back through the membranes. Effective backflushing is obtained by using high counterpressures

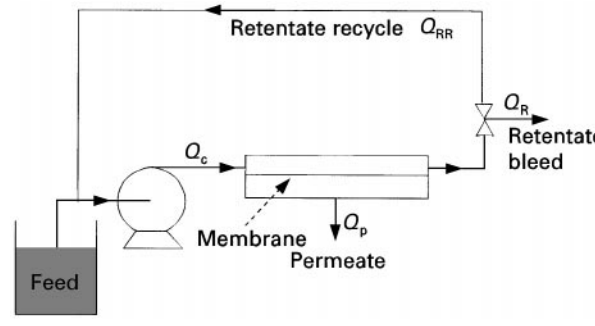

Figure 11 Feed-and-bleed operational configuration for cross-flow microfiltration.

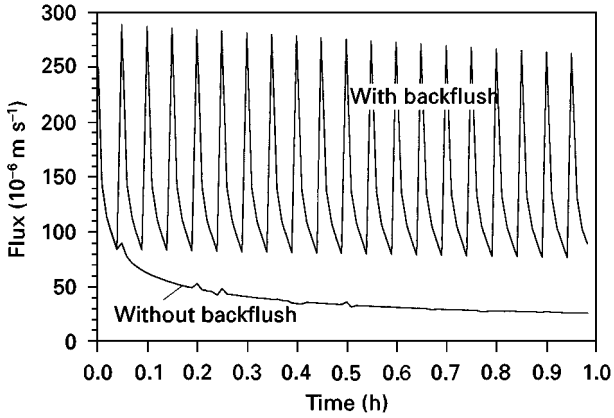

Figure 12 Microfiltration flux when filtering a particle suspension, with and without backflush.

(about 0.5 bar) for several seconds every few minutes (**Figure 12**).

Fouling is reduced by high cross-flow velocities and low transmembrane pressures. High cross-flow velocities cause high-pressure drops along the membrane, which cause the ΔP to be undesirably high at the entrance of the membrane module. Therefore microfiltration processes have been developed which facilitate a cross-flow both on the feed side and on the permeate side. The pressure drops on both sides are similar in magnitude, guaranteeing a *uniform transmembrane pressure*. This method of operation has been shown to be effective in many dairy applications.

Other process techniques to reduce fouling are the use of pulsed flow, gas sparging, and electric or acoustic fields, and the use of flow geometries that create secondary flows or vortices resulting in high shear rates (e.g. the use of 'turbulence promoters' or curved channels).

Conclusions

Over the last 70 years, microfiltration has developed from a small specialized technology used only in laboratories to a multibillion dollar industry for separation and purification of liquid and gas streams. Especially since the 1980s, exciting new applications have become possible, due to improved membranes (for example, ceramics) and improved technologies (for example, backpulsing, uniform transmembrane pressure). Still, great challenges exist, for example in the processing of beverages, such as fruit juices, milk, and beer, where membrane fouling seriously impairs the economy of the process.

To overcome these problems, researchers and engineers are becoming increasingly interested in hybrid and combined processes. Combining microfiltration with good pre- and post-treatments or with other separation processes may result in better and more economic separations.

See also: **II/Membrane Separations:** Filtration.

Further Reading

Belfort G, Davis RH and Zydney AL (1994) The behavior of suspensions and macromolecular solutions in cross-flow microfiltration. *Journal of Membrane Science* 96: 1–58.

Bowen WR and Jenner F (1995) Theoretical descriptions of membrane filtration of colloids and fine particles: an assessment and review. *Advances in Colloid and Interface Science* 56: 141–200.

Ho WSW and Sirkar KK (1992) *Membrane Handbook*. New York: Van Nostrand Reinhold.

Howell JA, Sanchez V and Field RW (1993) *Membranes in Bioprocessing – Theory and application*, 1st edn. London: Chapman and Hall.

Mulder M (1992) *Basic Principles of Membrane Technology*, 1st edn. Dordrecht: Kluwer Academic Publishers.

Scott K (1995) *Handbook of Industrial Membranes*. Oxford: Elsevier Science.

Zeman LJ and Zydney AL (1996) *Microfiltration and Ultrafiltration. Principles and Applications*. New York: Marcel Dekker.

Pervaporation

H. E. A. Brüschke and N. P. Wynn,
Sulzer Chemtech GmbH, Neunkirchen, Germany

Development

In 1917 PA Kober published a paper in which he described his observation that 'a liquid in a collodion bag, which was suspended in the air, evaporated, although the bag was tightly closed'. Kober was not the first researcher to observe this phenomenon, but the first to realize its potential for the separation of liquid mixtures which otherwise are difficult to separate, and to separate them under moderate conditions. He introduced the terms 'Pervaporation', and 'Perstillation', and the first term is now in use to describe in